The Cryosphere Discuss., 7, 2119–2151, 2013
www.the-cryosphere-discuss.net/7/2119/2013/
doi:10.5194/tcd-7-2119-2013

The Cryosphere Discussions
Open Access

Monitoring water accumulation in a glacier using magnetic resonance imaging

A. Legchenko[1], C. Vincent[2], J. M. Baltassat[3], J. F. Girard[3], E. Thibert[4], O. Gagliardini[2,6], M. Descloitres[1], A. Gilbert[2], S. Garambois[5], A. Chevalier[1], and H. Guyard[1]

[1]IRD/UJF-Grenoble 1/CNRS/G-INP, LTHE UMR5564, BP 53, Grenoble Cedex 9, 38041, France
[2]Laboratoire de Glaciologie et Géophysique de l'Environnement and CNRS – LGGE, 38041 Grenoble Cedex 9, France
[3]BRGM, BP 6009, 45060, Orléans Cedex 2, France
[4]IRSTEA, UR ETGR, BP 76, 38402 Saint-Martin-d'Hères Cedex, France
[5]Institut des Sciences de la terre (ISTerre), CNRS/ Université Joseph Fourier, Grenoble, France
[6]Institut Universitaire de France, IUF, Paris, France

Received: 29 March 2013 – Accepted: 17 May 2013 – Published: 31 May 2013

Correspondence to: A. Legchenko (anatoli.legtchenko@ird.fr)

Published by Copernicus Publications on behalf of the European Geosciences Union.

Abstract

Tête Rousse is a small polythermal glacier located in the Mont Blanc area (French Alps) at an altitude of 3100 to 3300 m. Recent accumulation of melt water in the glacier was assumed to occur, but such accumulation had yet to be confirmed. Using Surface Nuclear Magnetic Resonance imaging (3-D-SNMR), we showed that the temperate part of the Tête Rousse glacier contains two separate water-filled caverns (central and upper caverns). In 2009, the central cavern contained about 55 000 m^3 of water. Since 2010, the cavern is drained every year. Using 3-D-SNMR, we monitored the changes caused by this pumping in the water distribution within the glacier body. Twice a year, we carried out magnetic resonance imaging of the entire glacier and estimated the volume of water accumulated in the central cavern. Our results show the changes in cavern geometry and recharge rate: in two years, the central cavern lost about 73 % of its initial volume, but 65 % were lost in one year after the first pumping. We also observed that, after being drained, the cavern was recharged at an average rate of 20 to 25 $m^3\,d^{-1}$ over the winter months and 120 to 180 $m^3\,d^{-1}$ in summer. These observations illustrate how ice and water may refill englacial volume being emptied by artificial draining. Comparison of the 3-D-SNMR results with those obtained by drilling and pumping showed a very good correspondence, confirming the high reliability of 3-D-SNMR imaging.

1 Introduction

Water circulation in a glacier is an important factor that determines ice dynamics, runoff characteristics, and water quality. The recent, growing, concern over the response of glaciers to future-climate scenarios necessitates recognition of the hydrological processes in ice. A significant proportion of glaciers exhibit a polythermal regime, where ice masses are composed of temperate ice (at the pressure melting point) and cold ice (Irvine-Fynn et al., 2011). In a polythermal glacier, the coexistence of temperate and

TCD
7, 2119–2151, 2013

cold ice increases the potential for water storage within the glacier's drainage system. Observations at Austre Brøggerbreen in 1998 and 2000 showed that a water volume of approximately 8000 m^3 was retained in a single englacial channel (Schroeder, 1998). At Hansbreen, the annual water volumes in englacial conduits were estimated to be about 1.3×10^6 m^3 (Benn et al., 2009). However, the total volume of accumulated water will depend upon channel density and dimensions, glacier size, and the rate at which summer-season outflow is curtailed. Water trapped within a glacier can lead to extreme discharge events (Haeberli, 1983; Jansson et al., 2003). In densely populated mountain areas, glaciers may affect a number of hazard-relevant issues, such as abrupt floods (Haeberli et al., 1989) or slope instability (Fischer et al., 2005). A better understanding of hydrological processes taking place in polythermal glaciers and the design of suitable protection measures against new hazards requires regular observations and detailed knowledge of the internal glacier structure, which can be obtained using surface geophysical methods.

In recent years, ground-penetrating radar (GPR) has been increasingly used for the definition of subglacial and englacial environments (Irvine-Fynn et al., 2006; Bælum and Benn, 2011). Using calibrations and additional temperature data, GPR helped estimating the water content in the ice (Hamran et al., 1996; Macheret and Glazovsky, 2000), and more recent GPR research examined temporal changes in glaciers and investigation of 2-D and 3-D structures (Grasmueck et al., 2004; Gross et al., 2004). Reported study of ice properties by combining surface and borehole radar measurements improves the accuracy of the results (Murray et al., 2000). Other non-invasive methods, like seismic techniques (Lanz et al., 1998; Musil et al., 2002; Maurer and Hauck, 2007), frequency- and time-domain electromagnetic methods (FDEM and TDEM, respectively) (Hoekstra, 1978; Hauck et al., 2001) and electrical resistivity tomography (ERT) (Hauck and Vonder Mühll, 2003; Marescot et al., 2003; Kneisel, 2004) provide both redundant and complementary information about glacier features. Joint interpretation of data obtained with different methods provides more reliable and accurate results (Endres et al., 2009; Kim et al., 2010; Merz et al., 2012). However, variations in

TCD
7, 2119–2151, 2013

the physical parameters of the investigated formations observed by these traditional geophysical methods do not allow a unique interpretation in terms of water presence and hence an estimate of the water volume accumulated in a glacier body can only be qualitative.

In this paper, we report our results of using the Surface Nuclear Magnetic Resonance method (SNMR), also known as the Magnetic Resonance Sounding (MRS), for investigating hydrological processes in a glacier. SNMR is an emerging geophysical technique, specifically developed for hydrogeological investigations (Legchenko and Valla, 2002; Hertrich, 2008; Knight et al., 2012). Selective sensitivity to groundwater is the main advantage of SNMR in comparison with other geophysical tools, and the magnetic resonance phenomenon can also be used for investigating brine inclusions of Antarctic sea ice (Callaghan et al., 1999). Cold ice with negligible interstitial water does not produce an SNMR response and hence is interpreted as a dry material. On the contrary, temperate ice may contain liquid water and SNMR can quantify this water content. In its 2-D and 3-D implementation, SNMR was reported to be an efficient method for investigating subglacial formations (Lehmann-Horn et al., 2011) and for locating water-filled caverns and channels in a karst environment (Vouillamoz et al., 2003; Boucher et al., 2006; Girard et al., 2007; Legchenko et al., 2008). For 2-D and 3-D investigations, SNMR can be used with separate transmitting (Tx) and receiving (Rx) loops (Hertrich et al., 2009), or with a coincident Tx/Rx loop (Legchenko et al., 2011). We used the coincident Tx/Rx loop configuration as being better adapted to the high mountain conditions.

As part of our research, we have studied the Tête Rousse glacier located in the Mont Blanc area (French Alps). Tête Rousse being a polythermal glacier, our results can be taken into account when investigating other glacial environments.

TCD
7, 2119–2151, 2013

2 3-D-SNMR method: background

The SNMR field setup consists of a wire loop laid out on the surface, usually in a square with sides between 40 and 150 m. The loop is then energized by a pulse of alternating current $i(t) = I_0 \cos(\omega_0 t)$. The current frequency is set equal to the Larmor frequency of the protons ω_0 in the geomagnetic field B_0 ($\omega_0 = \gamma B_0$ with γ being the gyromagnetic ratio). The pulse causes precession of the spin magnetization of the protons in groundwater around the geomagnetic field, which creates an alternating magnetic field that can be detected by the same loop after the pulse is terminated (the free-induction decay method). Oscillating at the Larmor frequency, the SNMR signal is measured by varying the pulse moment $q = I_0 \tau$, with I_0 and τ being the amplitude and duration of the pulse, respectively. The distribution of the water content in the subsurface can be derived from the inversion of the SNMR signal.

The signal induced in the coincident transmitting/receiving (Tx/Rx) loop is proportional to the sum of the flux of all precessing magnetic moments and can be computed with the volume integral (Valla and Legchenko, 2002):

$$e_0(q) = I_0^{-1} \omega_0 \int_V B_1 M_\perp w(\mathbf{r}) \mathrm{d}V, \quad (1)$$

where $M_\perp = \sin(\gamma B_1 I_0^{-1} q/2)$ is the transverse component of spin magnetization, γ is the gyromagnetic ratio, B_1 is transmitted by the surface-loop magnetic-field component perpendicular to the geomagnetic field, I_0 is the current amplitude in the loop, q is the pulse moment, I_0 is the Larmor frequency for protons in the geomagnetic field, $0 \le n(\mathbf{r}) \le 1$ is the water content, and $\mathbf{r} = r(x, y, z)$ is the coordinate vector.

The 3-D implementation of the method consists of overlapping Tx/Rx loops. The SNMR signal is independently measured in each loop while varying the pulse moment. All individual soundings are incorporated into one data set for the 3-D inversion (Legchenko et al., 2011). For the inversion, the linear Eq. (1) is approximated by

TCD
7, 2119–2151, 2013

a matrix equation

$$\mathbf{Aw} = \mathbf{e}, \tag{2}$$

where $\mathbf{A} = [\tilde{a}_{i,j}]$ is a rectangular matrix with the elements that represent the amplitude of the magnetic-resonance signal generated by water in corresponding cells. The experimental data set is $\mathbf{e} = (\tilde{e}_1, \tilde{e}_2, ..., \tilde{e}_i, \tilde{e}_I)^T$, the water content in the corresponding cell is $\mathbf{w} = (w_1, w_2, ..., w_j, ..., w_J)^T$, and the symbol T denotes the transposition. For simplicity, we assume that cell size is constant throughout the investigated volume.

Inversion of the 3-D-SNMR data is ill-posed. Different methods for resolving ill-conditioned inverse problems can be found in the literature (Tarantola, 1987). For our study, the inversion was conducted according to Tikhonov's regularization method (Tikhonov and Arsenin, 1977). To find an approximate solution to the matrix Eq. (2), this method supposes minimization of Tikhonov's functional (Legchenko and Shushakov, 1998):

$$\mathrm{TF}(\eta) = \| \mathbf{Aw} - \mathbf{e} \|_{L_2} + S_{x,y,z} = \min, \tag{3}$$

where $S_{x,y,z} = \eta_x \times (\frac{\partial}{\partial x}\mathbf{w})^2 + \eta_y \times (\frac{\partial}{\partial y}\mathbf{w})^2 + \eta_Z \times (\frac{\partial}{\partial z}\mathbf{w})^2$ is an estimate of the smoothness of the solution and $\eta > 0$ are the smoothing factors in each direction. For the optimization itself, we used the conjugate gradient method (Stoer and Bulirsch, 1980).

Numerical modeling shows that 3-D-SNMR cannot resolve small targets and provides only results averaged over a volume larger than the target-volume. Thus, for small and/or deep targets, inversion shows a larger area with smaller water content and the water location will not be precisely known. However, it was shown that the signal amplitude generated by the same amount of water depends on the water position relative to the loop axis (Legchenko et al., 2011). Consequently, the water volume in small structures based on the unconstrained inversion results cannot be estimated, though the use of constrains may overcome the insufficient resolution of the inversion.

Another approach consists of estimating the water volume by forward modeling. 3-D inversion provides an approximate location of water in the glacier and allows easy

TCD
7, 2119–2151, 2013

forward modeling using a box model. The number, location and water content in each box are selected so that the theoretical signal, computed by considering the water in the boxes, fits the experimental data. Many equivalent models can be created with this approach, which allows investigating the solution space and thus provides access to the uncertainty in the 3-D-SNMR imaging. For example, for estimating the minimum and maximum possible amounts of water that can may explain the measured signals, we used water located in areas with preferably high and low sensitivities of the SNMR loops.

3 Investigated area

The area investigated with 3-D-SNMR is located in the French Alps (Fig. 1). Tête Rousse is a small glacier; in 2007 its surface area was about 0.08 km^2 (Fig. 2). A temperate accumulation area and a predominantly cold ablation area characterize the thermal regime of the Tête Rousse glacier. Reported results of numerical simulations of snow cover and englacial temperatures show that the glacier was almost entirely cold before 1870, but then gradually warmed up until 1920. In that year, the glacier was almost entirely temperate except for its central deeper part that remained cold. Between 1920 and 1950, the glacier started freezing again, but the temperate part remained large. Nowadays, except for the first ten meters close to the surface, influenced by seasonal temperature variations, the glacier consists of temperate and cold ice (Gilbert et al., 2012). In its western part, below 3160 m elevation, the glacier body is composed of cold ice with a temperature below −2 °C. Above 3180 m, the basal ice is temperate or near temperate in the first 10 to 20 m above bedrock. In the central part, between 3160 and 3180 m, the ice is temperate from approximately 30 m below the glacier surface down to bedrock (Vincent et al., 2012a). A large water-filled cavern containing about 55 000 m^3 of water was discovered in 2009 (Vincent et al., 2012b). Whatever the mechanism explaining the penetration of water into the glacier, this water reached the bottom and was trapped by the thermal barrier formed by cold basal ice. Therefore, the

TCD
7, 2119–2151, 2013

thermal regime could explain, at least in part, the storage of water within the glacier. In 1892, the outburst flood from this glacier released about 200 000 m^3 of water mixed with ice and caused much damage (Vallot et Delebecque, 1892; Mougin and Bernard, 1905; Vincent et al., 2010). Nowadays, about 3000 inhabitants are exposed to the Tête Rousse hazard and water in the cavity has therefore been pumped every fall since 2010.

4 Results

During our study, we used half-overlapping square loops ($80 \times 80\,m^2$) that covered the major part of the glacier (Fig. 2). The depth of investigation with this loop was about 80 m. Nine loops were used between 2009 and 2011 (black squares) and three additional loops were added for surveys carried out in 2012 (red squares). We used NUMIS^{plus} equipment manufactured by IRIS Instruments (France). Data processing and 3-D inversion were done with the SAMOVAR-11 × 4 software package developed in the *Institut de Recherche pour le Développement* (IRD, France).

4.1 3-D-SNMR measurements

Figure 2 shows the location of the central cavern as a horizontal slice at an elevation of 3124 m, corresponding to a depth of 46 m below the glacier surface. Note that the average water content given by 3-D-SNMR inversion is 40 % instead of the 100 % expected for bulk water in the cavern. This discrepancy can be explained by the limited resolution of magnetic resonance imaging, which shows an area larger than the true cavern with a water content averaged over this larger area. The water reservoir may also have a complex geometry unresolved by the inversion. We studied numerically the accuracy of 3-D-SNMR inversion under Tête Rousse glacier conditions. The results suggest an uncertainty in the target location as ±20 m and in the water volume estimate as ± 20 % (Legchenko et al., 2011).

TCD
7, 2119–2151, 2013

Figure 3 shows the amplitude of the SNMR signal versus pulse moment, measured with loop N°1 located over the central cavern (see Fig. 2 for location). The measurements were carried out at different periods, when the cavern contained different volumes of accumulated water. In all three cases, the measured SNMR signal was significantly larger than the ambient electromagnetic noise. The smaller signal thus corresponds to smaller volumes of water, which demonstrates the sensitivity of the method to water-volume variations.

4.2 Water volume estimate

Between 2010 and 2012, the central cavern was drained three times and once we performed 3-D-SNMR measurements during such pumping. A 3-D-SNMR survey carried out in June 2010 did not detect any changes in the water distribution between September 2009 and June 2010, and we assume that the 3-D-SNMR results obtained in 2009 can be compared with pumping results obtained in 2010. Thus, we have four points for comparing 3-D-SNMR estimates of the water volume and the volume extracted by pumping from this cavern. A summary of the measurements of the water volume accumulated in the central cavern using 3-D-SNMR and pumping is presented in Table 1. Figure 4 shows a linear correlation (dashed line) between the water volume estimated by 3-D-SNMR and that extracted by pumping.

Comparison with the pumping data shows that 3-D-SNMR consistently overestimated the volume of water relative that extracted by pumping. The average discrepancy between 3-D-SNMR and pumping was calculated as approximately 3100 m^3. At least some part of this volume can be attributed to the residual water remaining in the glacier after pumping, because technically it was impossible to extract all the water. Moreover, water in hydraulically disconnected caverns and channels contributes to the SNMR signal, but cannot be pumped out. Additionally, it is known that the water content in temperate ice usually varies between 0.7 % and 2.5 % (Lliboutry, 1976; Bradford et al., 2009) and may be as high as 9 % (Pettersson et al., 2004). This water will increase the SNMR signal, but only part of it can be pumped out.

TCD
7, 2119–2151, 2013

The location of the temperate ice in the Tête Rousse glacier was approximately known (Gilbert et al., 2012; Vincent et al., 2012b) and we estimated numerically its potential water volume. To this end, for areas occupied by temperate ice we added 2 % water content to the model of the water-filled cavern in the glacier body. Modeling results show that, in the Tête Rousse glacier, up to 2000 m^3 of the water volume measured by 3-D-SNMR may represent the contribution of water in temperate ice. However, the pumping operation took 44 days in 2010, 13 days in 2011 and 17 days in 2012, during which the cavern was continuously recharged. The recharge rate was unknown, but as snow melt on the Tête Rousse glacier in September–October is minimal the recharge can be assumed to be slightly higher than in winter (20 to 30 $m^3 d^{-1}$). Therefore, an additional water volume of 250 to 1200 m^3 can be expected in the cavern, which contributed to the pumping results but could not be taken into account by the 3-D-SNMR estimate. All these processes are difficult to quantify, but they cause additional inaccuracy of the volume estimate made by both 3-D-SNMR and pumping.

4.3 Monitoring

Twice a year, we carried out magnetic resonance measurements that allowed imaging about 75 % of the glacier body. Each 3-D-SNMR campaign provided a water distribution within the glacier and an estimate of the water volume. Measurements were made in early June, after winter recharge, and in September, after the summer recharge.

The central cavern, discovered in 2009, was the starting point of our monitoring. The 3-D image of the cavern (Fig. 5) shows the cavern location within the glacier. Through the regular 3-D-SNMR measurements, we obtained time-lapsed images of the cavern. For example, Fig. 5 shows the undisturbed cavern observed in 2009 and Fig. 6 shows the same cavern imaged in 2011 after one drainage-and-refilling cycle. Comparison of these images shows that the cavern remained in the same place, but that drainage caused changes in the cavern geometry and in the water-content distribution. In 2011, the maximum water content was estimated at 15 % instead of the 40 % observed in 2009, pointing to a smaller size and smaller volume of water in the cavern in 2011.

TCD
7, 2119–2151, 2013

To compare 3-D-SNMR and pumping results, a 3-D-SNMR image can be transformed into a 1-D plot of the water volume per unit depth for different elevations. For that, we performed integration in the X and Y directions of the 3-D water distribution $w(\mathbf{r})$, provided by the inversion (Eq. 1). The 3-D-SNMR and pumping results obtained between 2009 and 2012 are shown on Figs. 7 and 8. On Fig. 7, the volume of accumulated water derived from the 3-D-SNMR results is plotted versus depth and is compared with the volume of water extracted by pumping. We observe a generally good correspondence between 3-D-SNMR and pumping for the depth interval corresponding to the main cavern volume. However, at the bottom of the cavern, the correlation is not as good as for the shallow part, because of a more complex geometry of the deeper part of the cavern where 3-D-SNMR tends to overestimate the water volume due to processes exposed in Sect. 4.2. When the cavern was larger (2009–2011), the correlation was better than in 2012, probably because the cavern geometry became more complex after the first drainage. Figure 8 shows the water volume per unit depth versus depth derived from 3-D-SNMR and pumping results, which are the derivatives of the functions presented in Fig. 7. The correlation is generally good, but the rapid variations in extracted volume, observed by pumping, were not resolved by the 3-D-SNMR inversion. Figure 8 clearly shows that the main reservoir discovered in 2009 was located below 3125 m and that after the first drainage-and-refilling cycle this reservoir was significantly smaller. In 2012, we observed water only above 3125 m. A summary of the water volume monitoring is shown in Table 2.

4.4 Recharge of the central cavern

During our monitoring, the cavern was continuously recharged. The results of water volume measurements are shown on Fig. 9, which indicate that the water volume in the fully recharged cavern was reduced after each drainage-and-refilling cycle. In one year, the cavern lost about 65 % of its volume and in two years it was reduced by about 73 %. Note that in Tables 1 and 2 the water volume observed in 2012 (11 200 m^3) corresponds to water in the cavern that was drained, thus allowing comparison between

TCD
7, 2119–2151, 2013

3-D-SNMR and pumping. In Fig. 9, however, we consider all water observed in the glacier (14 500 m^3), also taking into account 3300 m^3 in a small cavern, which was imaged but was not affected by pumping.

For estimating the recharge rate, we used the 3-D-SNMR estimates of water volume. Regular magnetic resonance measurements were made in early June for estimating the winter recharge rate, and in August or September for estimating the summer recharge rate. The average recharge rate was estimated as:

$$Q_n = (V_{n+1} - V_n)/(t_{n+1} - t_n), \quad (4)$$

where V_n is the water volume in the cavern corresponding to the nth measurement, t_n is time, and $n = 0, 1, 2, ..., N$.

The average recharge rate observed between 2010 and 2012 is shown on Fig. 10. The summer recharge rate was estimated to be between 120 and 180 $m^3 d^{-1}$ and recharge continued throughout the winter with an average rate of 20–25 $m^3 d^{-1}$. We calculated the winter recharge rate by considering the volume of residual water left in the cavern after pumping, which was estimated as the difference between the water volume given by 3-D-SNMR before pumping and the volume of water extracted by pumping (Table 1).

To explain the winter recharge, when no melting occurs at the glacier surface, and only solid precipitation exists at this altitude, we looked for a water reservoir located at a higher elevation than the central cavern. For that, the measuring setup was extended towards the eastern part of the glacier (see Fig. 2 for location). The 3-D-SNMR image of the glacier obtained in 2012, using the additional loops (Fig. 11), in fact showed two distant reservoirs. The central reservoir is the cavern known from 2009; this became smaller in comparison with previous years and its maximum water content was only 5 % instead of the 15 % observed in 2011 and the 40 % in 2009. The second cavern (upper cavern) is located at about 150–200 m to the east of the central cavern and at a higher elevation, in a dangerous area with difficult access. For this reason, accurate 3-D-SNMR imaging of this cavern was not possible in 2012. The 3-D-SNMR estimate of

TCD
7, 2119–2151, 2013

the water volume in the upper cavern suggests over 5000 m^3, but this preliminary result requires further investigation. To verify the existence of a possible high-yield hydraulic link between the two caverns (tunnel or large channel), we made magnetic resonance measurements over the upper cavern before and immediately after the drainage of the central cavern. Results show that the 3-D-SNMR signal generated by water in the upper cavern did not change, thus confirming that, if the pumping affected the upper cavern, this was below the detection threshold of the instrument.

5 Discussion

The use of 3-D-SNMR allowed quantifying the temporal and spatial changes in water distribution caused by the annual draining of the water-filled cavern. During our experiments, we confirmed that the 3-D-SNMR method is a reliable and cost-effective tool for investigating water in a glacier. Unambiguous identification of liquid water in ice, localization of water storage areas, and the possibility of estimating the water volume stored in a glacier, are the main advantages of 3-D-SNMR compared with traditional geophysical methods. In a highly heterogeneous environment, non-invasive imaging of a large area allows visualizing the entire glacier, which is the competitive advantage of 3-D-SNMR over boreholes. Indeed, each borehole may be not representative, and the need for drilling many boreholes renders the fieldwork longer and more expensive (Gordon et al., 2002). Applied under glacier conditions, pumping may cause changes in the internal structure of the investigated glacier, but 3-D-SNMR is a non-destructive method. However, 3-D-SNMR and pumping are complementary techniques that provide close, but different, visions of glacier hydrology. For example, 3-D-SNMR detects and visualizes water, regardless of whether or not a hydraulic link exists between different areas, but pumping may provide information on the hydraulic connection of different reservoirs.

Figure 11 shows that water in the Tête Rousse glacier accumulated in two separate reservoirs (central and upper caverns). The upper cavern would be preferentially

TCD
7, 2119–2151, 2013

recharged by melt water, but the central cavern may accumulate both surface and englacial water with corresponding refilling rates. Our results show that a large tunnel does not directly connect these two caverns, but that water may flow from the upper cavern through a subglacial drainage system and probably through sub-glacial sediments with a relatively low hydraulic conductivity. This slow drainage would explain the observed continuous recharge of the central cavern during the winter months. In summer, higher water fluxes may cause englacial channels increasing their hydraulic conductivity (Raymond et al., 1995; Hubbard et al., 1995), as well as more water flow on the ice surface. Such increased water circulation may explain the higher summer recharge rate observed during our monitoring. However, the subglacial drainage system in the Tête Rousse glacier is still not well-known and different drainage mechanisms typical for a polythermal glacier may coexist (Fountain and Walder, 1998).

The possibility of a cavern roof collapse during pumping was not excluded (Gagliardini et al., 2011), but significant deformation of the glacier surface became visible only in July 2012. However, monitoring of the water accumulated in the glacier showed that each pumping caused the volume of water in the central cavern to diminish. Both 3-D-SNMR and pumping results reveal that in one year (2010–2011) the cavern lost about 90 % of the volume in its deeper part below 3125 m (Table 2). The relatively rapid rate of temperate ice deformation may explain these observations. For example, Reynaud (1987) observed a 60 % reduction in inactive, englacial conduit diameters at depths of about 100 m over a 20 day period.

Despite of the new knowledge about the Tête Rousse glacier that has been acquired over the past three years, we still have an incomplete understanding of the glacial-hydrological processes and of the glacier-ice dynamics. For example, while a cold-ice barrier may explain the formation of the central cavern, the existence of the upper cavern was not expected. We hope to continue our monitoring, leading to the precise location and size of the upper cavern that will complete our understanding of the glacier structure, and of the ice deformation processes taking place in the glacier.

TCD
7, 2119–2151, 2013

6 Conclusions

The annual drainage of a large cavern in the central part of the Tête Rousse glacier caused not revolutionary but evolutionary changes in the cavern geometry, providing us with a rare opportunity of studying the glacier's transitional regime imposed by pumping. Tête Rousse can thus be seen as a real-scale physical model of a polythermal glacier, providing useful data that contribute to a better understanding of the different processes taking place in this type of glacier.

Imaging of the water distribution in the Tête Rousse glacier showed two main water storage areas and allowed estimating the volume of accumulated water. We observed continuous cavern recharge both in summer and during the winter months. The summer recharge rate was estimated to be six to eight times higher than the winter recharge rate. Our monitoring results revealed significant changes in the internal structure of the glacier, caused by the artificial drainage. In one year, the cavern lost about 65 % (30 000 m^3) of its initial volume, which was explained by creep deformation of the surrounding ice after the drainage. These observations provided useful information to decision makers for developing protection measures to minimize the risk of a flood from the glacier.

For this study, we used a newly developed 3-D-SNMR imaging method that allowed visualizing the englacial water and estimating the volume of water accumulated within the Tête Rousse glacier. The 3-D-SNMR results were found to be in a good agreement with pumping results and other observations, thus confirming the high reliability and efficiency of 3-D-SNMR imaging. As far as we know, this is the first report of applying large-scale magnetic resonance imaging to monitoring water accumulation in a glacier.

Acknowledgements. The town of Saint-Gervais (France), Service de Restauration des Terrains en Montagne (RTM), and the Préfecture de la Haute Savoie (France) funded this study. We thank N. Karr, F. Charles and V. Tairraz for useful advice and for taking part in collecting the field measurements. We also thank all the people who assisted us during this work.

TCD
7, 2119–2151, 2013

[2mm]
[3.5mm] The publication of this article is financed by CNRS-INSU.

References

Bælum, K. and Benn, D. I.: Thermal structure and drainage system of a small valley glacier (Tellbreen, Svalbard), investigated by ground penetrating radar, The Cryosphere, 5, 139–149, doi:10.5194/tc-5-139-2011, 2011.

Benn, D., Gulley, J., Luckman, A., Adamek, A., and Glowacki, P. S.: Englacial drainage system formed by hydrologically driven crevasse propagation, J. Glaciol., 55, 513–523, 2009.

Boucher, M., Girard, J. F., Legchenko, A., Baltassat, J. M., Dörfliger, N., and Chalikakis, K.:, Using magnetic resonance soundings to locate a water-filled karst conduit, J. Hydrol., 330, 413–421, 2006.

Bradford, J. H., Nichols, J., Mikesell, T. D., and Harper, J. T.: Continuous profiles of electromagnetic wave velocity and water content in glaciers: an example from Bench Glacier, Alaska, USA, Ann. Glaciol., 50, 1–9, 2009.

Callaghan, P. T., Dykstra, R., Eccles, C. D., Haskell, T. G., and Seymour, J. D.: A nuclear magnetic resonance study of Antarctic sea ice brine diffusivity, Cold Reg. Sci. Technol., 29, 153–171, 1999.

Endres, A. L., Murray, T., Booth, A. D., and West, L. J.: A new framework for estimating englacial water content and pore geometry using combined radar and seismic wave velocities, Geophys. Res. Lett., 36, L04501, doi:10.1029/2008GL036876, 2009.

Fischer, L., Kääb, A., Huggel, C., and Nötzli, J.: Geology, glacier changes, permafrost and related slope instabilities in a high-mountain rock face: Monte Rosa east face, Italian Alps, Geophys. Res. Abstr., 7, 00518, SRef-ID: 1607-7962/gra/EGU05-A-00518, 2005.

Fountain, A. G. and Walder, J. S.: Water flow through temperate glaciers, Rev. Geophys., 36, 299–328, 1998.

TCD
7, 2119–2151, 2013

Gagliardini, O., Gillet-Chaulet, F., Durand, G., Vincent, C., and Duval, P.: Estimating the risk of glacier cavity collapse during artificial drainage: the case of Tête Rousse Glacier, Geophys. Res. Lett., 38, L10505, doi:10.1029/2011GL047536, 2011.
Gilbert, A., Vincent, C., Wagnon, P., Thibert, E., and Rabatel, A.: The influence of snow cover thickness on the thermal regime of Tête Rousse Glacier (Mont Blanc range, 3200 m a.s.l.): consequences for outburst flood hazards and glacier response to climate change, J. Geophys. Res., 117, F04018, doi:10.1029/2011JF002258, 2012.
Girard, J. F., Boucher, M., Legchenko, A., and Baltassat, J. M.: 2-D magnetic resonance tomography applied to karstic conduit imaging, J. Appl. Geophys., 63, 103–116, 2007.
Gordon, S., Sharp, M., Hubbard, B., Willis, I., Smart, C., Copland, L., Harbor, J., and Ketterling, B.: Borehole drainage and its implications for the investigation of glacier hydrology: experiences from Haut Glacier d'Arolla, Switzerland, Hydrol. Process., 15, 797–813, 2001.
Grasmueck, M., Weger, R., and Horstmeyer, H.: Three-dimensional ground-penetrating radar imaging of sedimentary structures, fractures, and archaeological features at submeter resolution, Geology, 32, 933–936, 2004.
Gross, R., Green, A. G., Horstmeyer, H., and Begg, J. H.: Location and geometry of the Wellington Fault (New Zealand) defined by detailed three-dimensional georadar data, J. Geophys. Res., 109, B05401, doi:10.1029/2003JB002615, 2004.
Hamran, S.-E., Aarholt, E., Hagen., J. O., and Mo, P.: Estimation of relative water content in a sub-polar glacier using surface-penetration radar, J. Glaciol., 42, 533–537, 1996.
Haeberli, W.: Frequency and characteristics of glacier floods in the Swiss Alps, Ann. Glaciol., 4, 85–90, 1983.
Haeberli, W., Alean, J. C., Müller, P., and Funk, M.: Assessing risks from glacier hazards in high mountain regions: some experiences in the Swiss Alps, Ann. Glaciol., 13, 96–102, 1989.
Hauck, C. and Vonder Mühll, D.: Using DC resistivity tomography to detect and characterise mountain permafrost, Geophys. Prosp., 51, 273–284, 2003.
Hauck, C., Guglielmin, M., Isaksen, K., and Vonder Mühll, D.: Applicability of frequency domain and time-domain electromagnetic methods, Permafrost Periglac., 12, 39–52, 2001.
Hertrich, M.: Imaging of groundwater with nuclear magnetic resonance, Prog. Nucl. Mag. Res. Sp., 53, 227–48, 2008.
Hertrich, M., Green, A. G., Braun, M., and Yaramanci, U.: High-resolution surface NMR tomography of shallow aquifers based on multioffset measurements, Geophysics, 74, G47–G59, 2009.

TCD
7, 2119–2151, 2013

Hoekstra, P.: Electromagnetic methods for mapping shallow permafrost, Geophysics, 43, 782–787, 1978.
Hubbard, B. P., Sharp, M. J., Willis, I. C., Nielsen, M. K., and Smart, C. C.: Borehole water-level variations and the structure of the subglacial hydrological system of Haut Glacier d'Arolla, Valais, Switzerland, J. Glaciol., 41, 572–583, 1995.
Irvine-Fynn, T. D. L., Moorman, B. J., Williams, J. L. M., and Walter, F. S. A.: Seasonal changes in groundpenetrating radar signature observed at a polythermal glacier, Bylot Island, Canada, Earth Surf. Process. Landf., 31, 892–909, 2006.
Irvine-Fynn, T. D. L., Hodson, A. J., Moorman, B. J., Vatne, G., and Hubbard, A. L.: Polythermal glacier hydrology: a review, Rev. Geophys., 49, RG4002, doi:10.1029/2010RG000350, 2011.
Jansson, P., Hock, R., and Schneider, T.: The concept of glacier storage: a review, J. Hydrol., 282, 116–129, 2003.
Kim, K. Y., Lee, J., Hong, M. H., Hong, J. K., Jin, Y. K., and Shon, H.: Seismic and radar investigations of Fourcade Glacier on King George Island, Antarctica, Polar Res., 29, 298–310, 2010.
Kneisel, C.: New insights into mountain permafrost occurrence and characteristics in glacier forefields at high altitude through the application of 2-D resistivity imaging, Permafrost Periglac., 15, 221–227, 2004.
Knight, R., Grunewald, E., Irons, T., Dlubac, K., Song, Y., Bachman, H. N., Grau, B., Walsh, D., Abraham, J. D., and Cannia, J.: Field experiment provides ground truth for surface nuclear magnetic resonance measurement, Geophys. Res. Lett., 39, L03304, doi:10.1029/2011GL050167, 2012.
Lanz, E., Maurer, H. R., Green, A. G., and Ansorge, J.: Refraction tomography over a buried waste disposal site, Geophysics, 63, 1414–1433, 1998.
Legchenko, A. V. and Shushakov, O. A.: Inversion of surface NMR data, Geophysics, 63, 75–84, 1998.
Legchenko, A. and Valla, P.: A review of the basic principles for proton magnetic resonance sounding measurements, J. Appl. Geophys., 50, 3–19, 2002.
Legchenko, A., Ezersky, M., Camerlink, C., Al-Zoubi, A., Chalikakis, K., and Girard, J. F.: Locating water-filled karst caverns and estimating their volume using magnetic resonance soundings, Geophysics, 73, 51–61, 2008.

TCD
7, 2119–2151, 2013

Legchenko, A., Descloitres, M., Vincent, C., Guyard, H., Garambois, S., Chalikakis, K., and Ezerski, M.: Three-dimensional magnetic resonance imaging for groundwater, New J. Phys., 13, 025022, doi:10.1088/1367-2630/13/2/025022, 2011.
Lehmann-Horn, A., Walbrecker, J. O., Hertrich, M., Langston, G., McClymont, A. F., and Green, A. G.: Imaging groundwater beneath a rugged proglacial moraine, Geophysics, 76, B165–B172, 2011.
Lliboutry, L.: Physical processes in temperate glaciers, J. Glaciol., 16, 151–158, 1976.
Macheret, Y. Y., and Glazovsky, A. F.: Estimation of absolute water content in Spitsbergen glaciers from radar sounding data, Polar Res., 19, 205–216, 2000.
Marescot, L., Loke, M. H., Chapellier, D., Delaloye, R., Lambiel, C., and Reynard, E.: Assessing reliability of 2-D resistivity imaging in permafrost and rock glaciers using the depth of investigation index method, Near Surf. Geophys., 1, 57–67, 2003.
Maurer, H. and Hauck, C.: Instruments and Methods Geophysical imaging of alpine rock glaciers, J. Glaciol., 53, 110–120, 2007.
Merz, K. J., Maurer, H. R., Rabenstein, L., Buchli, T., and Springman, S. M.: Geophysical characterization of unstable permafrost in the Turtmann Valley, Switzerland, Geophys. Res. Abstr., 14, EGU2012-2107, 2012.
Mougin, P. and Bernard, C.: Études exécutées au glacier de Tête Rousse, in: Annales de l'Observatoire météorologique, physique et glaciaire du Mont Blanc (altitude 4,358 mètres), edited by: Vallot, J., Tome VI. G. Steinheil, Paris, 137–174, 1905.
Murray, T., Stuart, G. W., Fry, M., Gamble, N. H., and Crabtree, D. M.: Englacial water distribution in a temperate glacier from surface and borehole radar velocity analysis, J. Glaciol., 46, 389–398, 2000.
Musil, M., Maurer, H., Green, A. G., Horstmeyer, H., Nitsche, F. O., Vonder Mühill, D., and Springman, S.: Shallow seismic surveying of an Alpine rock glacier, Geophysics, 67, 1701–1710, doi:10.1190/1.1527071, 2002.
Pettersson, R., Jansson, P., and Blatter, H.: Spatial variability in water content at the cold-temperate transition surface of the polythermal Storglaciären, Sweden, J. Geophys. Res., 109, F02009, doi:10.1029/2003JF000110, 2004.
Raymond, C. F., Benedict, R., Harrison, W., Echelmeyer, K., and Sturm, M.: Hydrological discharges and motion of Fels and Black Rapids Glaciers, Alaska, USA: implications for the structure of their drainage systems, J. Glaciol., 41, 290–304, 1995.

TCD
7, 2119–2151, 2013

Reynaud, L.: The November 1986 survey of the Grand Moulin on the Mer de Glace, Mont Blanc Massif, France, J. Glaciol., 33, 130–131, 1987.
Schroeder, J.: Hans glacier moulins observed from 1988 to 1992, Svalbard, Norsk Geogr. Tidsskr., 52, 79–88, 1998.
Stoer, J. and Bulirsch, R.: Introduction to Numerical Analysis, Springer-Verlag, Berlin, 1980.
Tarantola, A.: Inverse problem theory. Methods for data fitting and model parameter estimation, Elsevier Science Publ. Co., Inc., New York, NY, USA, 1987.
Tikhonov, A. and Arsenin, V.: Solution of Ill-Posed Problems, John Wiley & Sons, Inc., New York, 1977.
Valla, P. and Legchenko, A.: One-dimensional modelling for proton magnetic resonance sounding measurements over an electrically conductive medium, J. Appl. Geophys., 50, 217–229, 2002.
Vallot, J. and Delebecque, A.: Sur les causes de la catastrophe survenue à Saint-Gervais (Haute Savoie), Compt. Rend. Acad. Sci., 115, 264–266, 1892.
Vincent, C., Garambois, S., Thibert, E., Lefèbvre, E., Le Meur, E., and Six, D.: Origin of the outburst flood from Tête Rousse glacier in 1892 (Mont-Blanc area, France), J. Glaciol., 56, 688–698, 2010.
Vincent, C., Descloitres, M., Garambois, S., Legchenko, A., Guyard, H., Lefebvre, E., and Gilbert, A.: Detection of a subglacial lake in Glacier de Tete Rousse (Mont Blanc area, France), J. Glaciol., 58, 866–878, 2012a.
Vincent, C., Descloitres, M., Garambois, S., Legchenko, A., Guyard, H., Thibert, E., Gilbert, A., Karr, N., and Tairraz, V.: Détection d'une poche d'eau au glacier de Tête Rousse en 2010 et mesures préventives pour éviter une catastrophe, La Houille Blanche, 2, 34–41, 2012b.
Vouillamoz, J. M., Legchenko, A., Albouy, Y., Bakalowicz, M., Baltassat, J. M., and Al-Fares, W.: Localization of saturated karst aquifer with magnetic resonance sounding and resistivity imagery, Ground Water, 41, 578–587, 2003.

TCD
7, 2119–2151, 2013

Table 1. Summary of measurements of the water volume accumulated in the central cavern using 3-D-SNMR and pumping.

Action	Schedule									
	5–16 Sep 2009	26 Aug–15 Oct 2010	25–28 Sep 2010	28 Sep–15 Oct 2010	3–9 Jun 2011	22–24 Sep 2011	26 Sep–9 Oct 2011	22–24 Jun 2012	14–22 Aug 2012	24 Sep–8 Oct 2012
3-D-SNMR volume (m^3)	53 500		19 500		7000	18 500		8500	11 200	
Pumped volume (m^3)		47 728		17 362			16 162			8904
Discrepancy (m^3)		5572		2138			2338			2296
Discrepancy (%)		10.8		11			12.6			20.5

TCD
7, 2119–2151, 2013

Table 2. Summary of the 3-D-SNMR and pumping estimates of the changes in water volume in the central cavern caused by drainage. Evolution of the volume was estimated relative the initial volume observed in 2010.

Method	Depth interval (m)	2010 (m^3)	2011 (m^3)	2012 (m^3)	Evolution 2010–2011 (%)	Evolution 2011–2012 (%)
Pumping	3170–3125	13 617	13 663	8464	0.3	−38.2
	3125–3095	34 111	2499	440	−92.7	−6.0
	3170–3095	47 728	16 162	8904	−66.1	−15.2
3-D-SNMR	3170–3125	10 600	11 700	10 800	10.4	−8.5
	3125–3095	42 900	6800	400	−84.1	−14.9
	3170–3095	53 500	18 500	11 200	−65.4	−13.6

TCD
7, 2119–2151, 2013

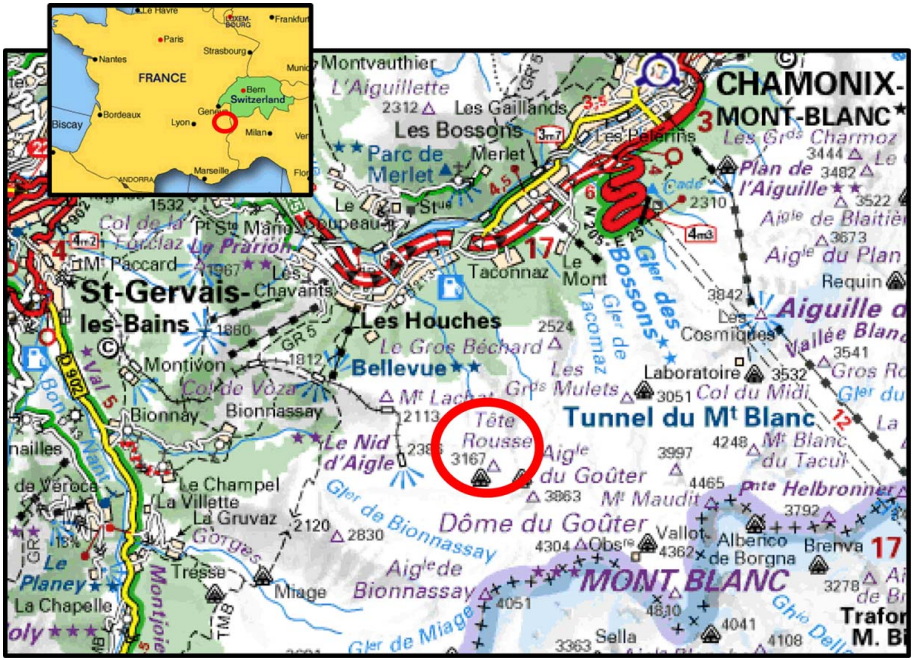

Fig. 1. Location of the Tête Rousse glacier.

TCD
7, 2119–2151, 2013

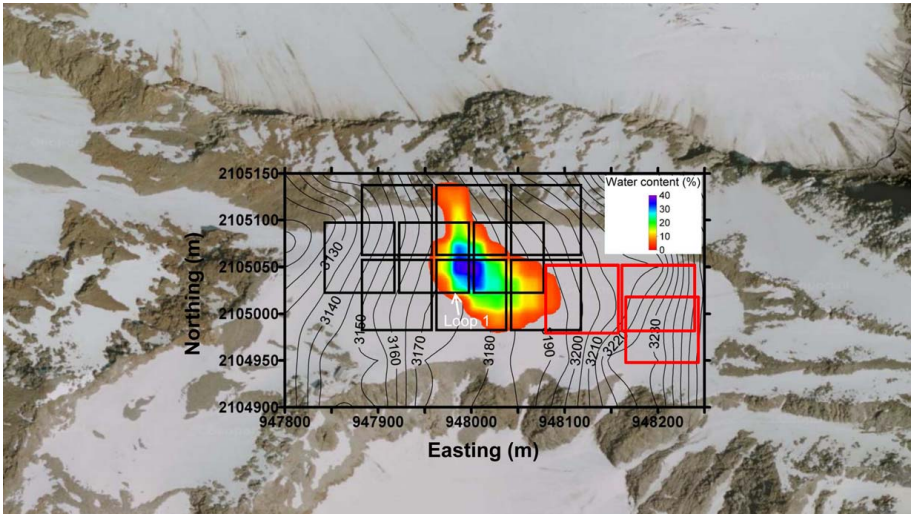

Fig. 2. Aerial photo of the Tête Rousse glacier with an approximate projection of the SNMR measuring loops (black squares) and water-filled cavern detected in 2009 (in the Lambert-II co-ordinate system). Additional SNMR loops used in 2012 are shown as red squares. Isoclines show the elevation of the glacier surface in 2009.

TCD
7, 2119–2151, 2013

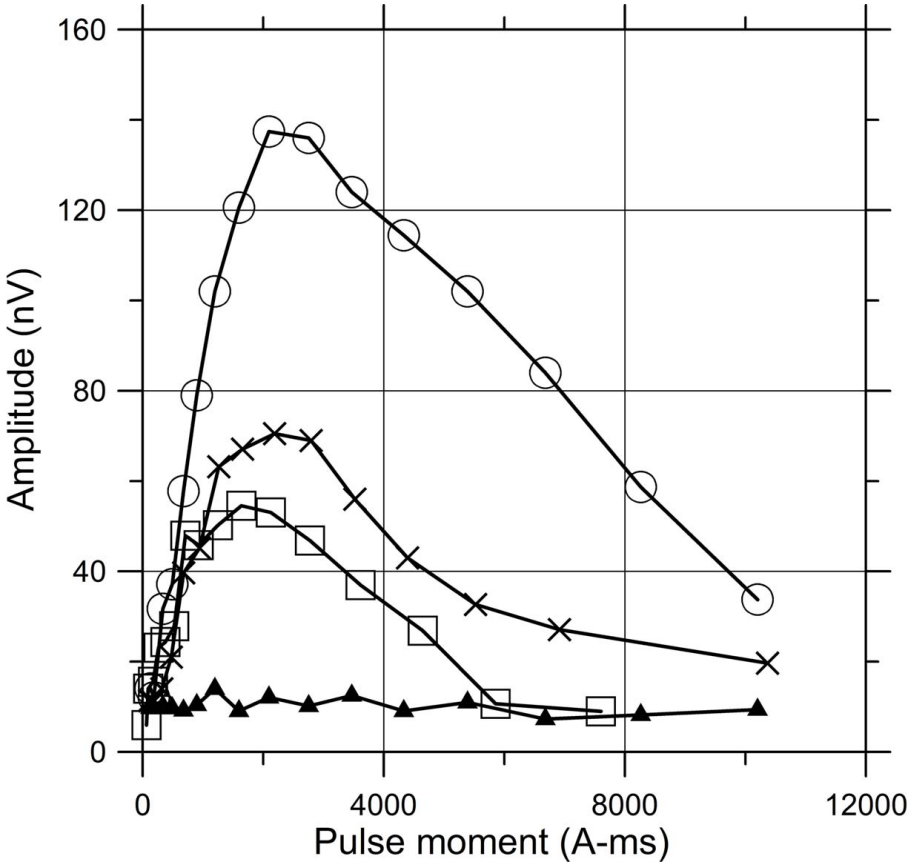

Fig. 3. Amplitude of the SNMR signal versus pulse moment measured with the loop N°1. Circles show the amplitude measured in 2009 when the cavern was undisturbed by pumping (V = 53 500 m^3), crosses correspond to 2011 data (V = 18 500 m^3) and squares present measurements in 2012 (V = 11 200 m^3). Triangles show measurements of the ambient electromagnetic noise.

TCD
7, 2119–2151, 2013

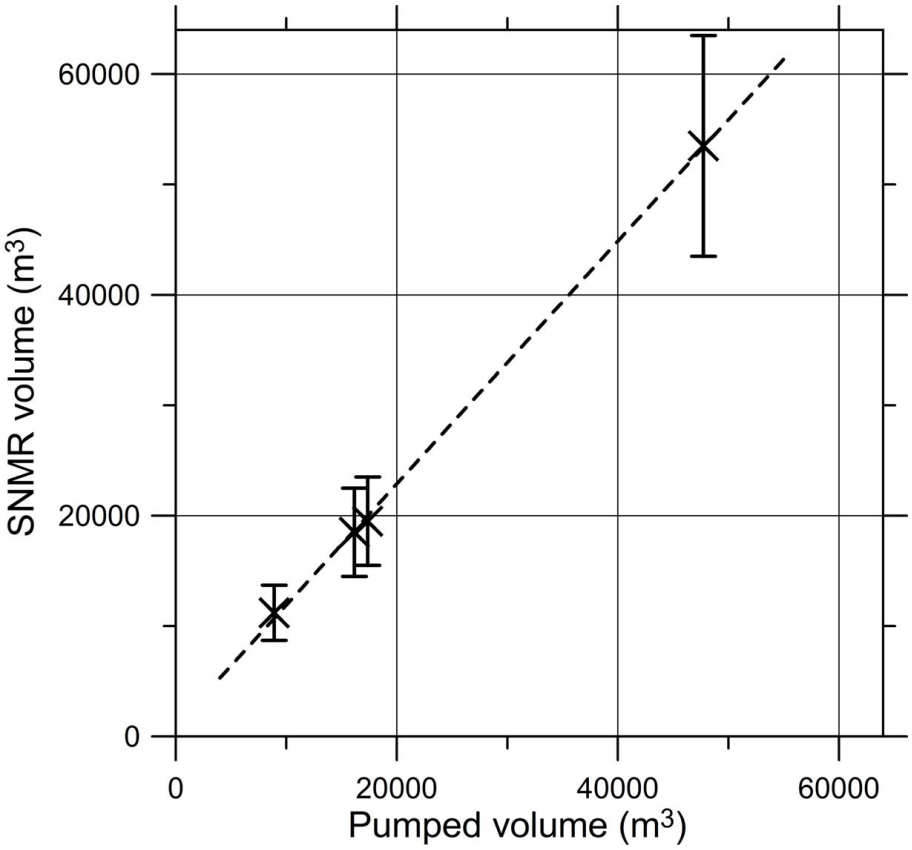

Fig. 4. 3-D-SNMR water volume estimated before each pumping against the water volume extracted by pumping. The dashed line shows the linear fit.

TCD
7, 2119–2151, 2013

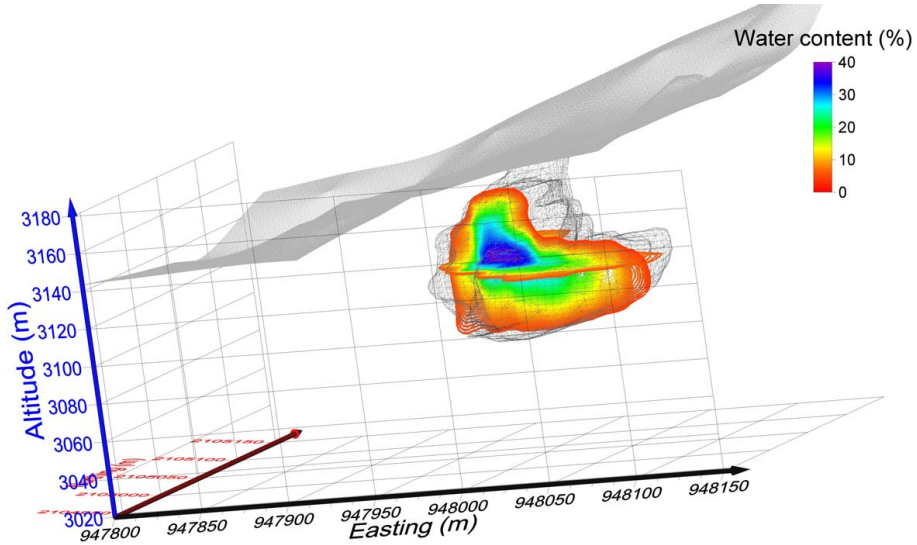

Fig. 5. 3-D-SNMR image of the water-filled cavern observed in September 2009. The glacier surface is shown as a gray sheet.

TCD
7, 2119–2151, 2013

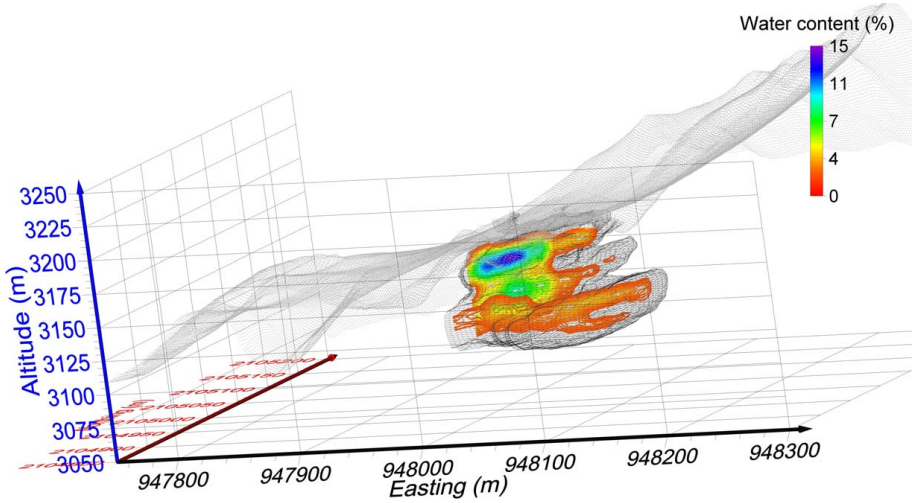

Fig. 6. 3-D-SNMR image of the water-filled cavern observed in September 2011. The glacier surface is shown as a gray sheet.

TCD
7, 2119–2151, 2013

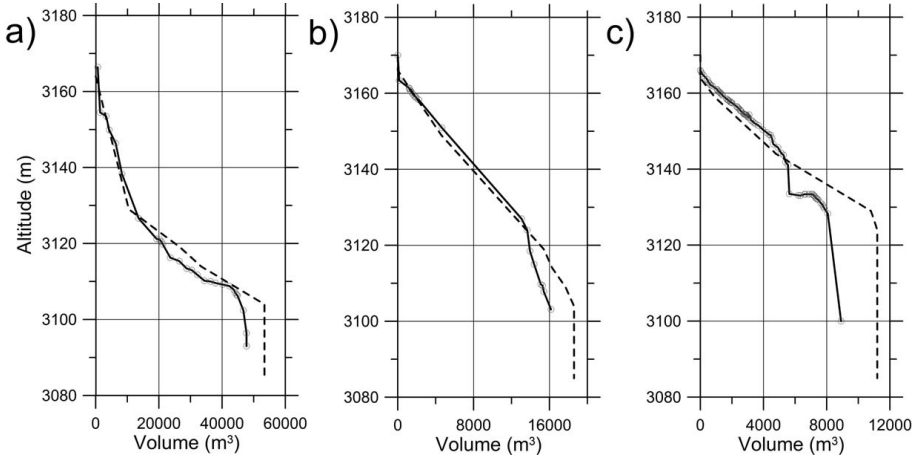

Fig. 7. Accumulated water volume versus depth extracted by pumping (solid line) and the water volume estimated with the 3-D-SNMR (dashed line): **(a)** August–October 2010, **(b)** September–October 2011, **(c)** August 2012.

TCD
7, 2119–2151, 2013

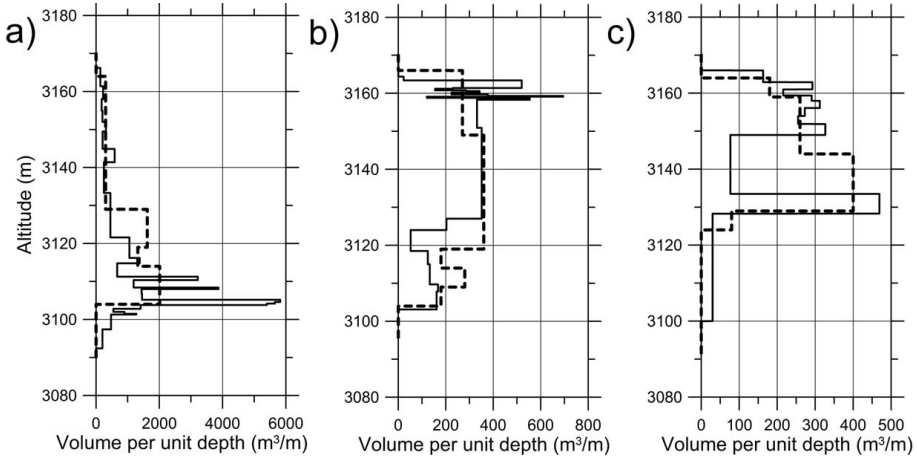

Fig. 8. Water volume per unit depth extracted from different depth intervals (solid line) and the water volume per unit depth estimated with the 3-D-SNMR (dashed line): **(a)** August–October 2010, **(b)** September–October 2011, **(c)** August 2012.

TCD
7, 2119–2151, 2013

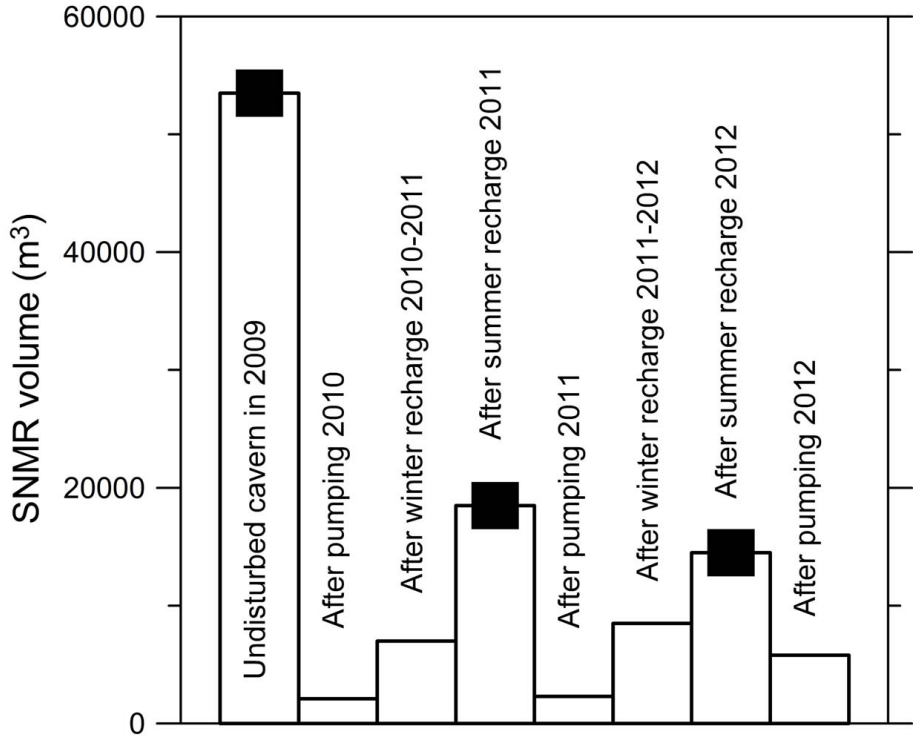

Fig. 9. Monitoring of the water volume accumulated in the central part of the Tête Rousse glacier between 2009 and 2012. Black squares show the volume after full recharge.

TCD
7, 2119–2151, 2013

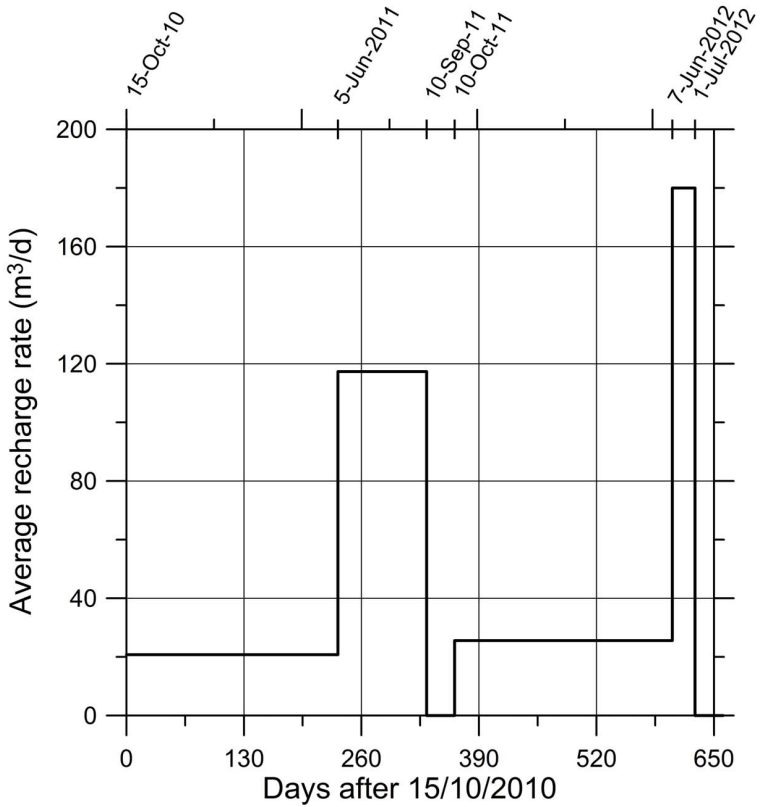

Fig. 10. Estimated average recharge rate of the cavern in the Tête Rousse glacier for the period between 15 October 2010 and 1 August 2012.

TCD
7, 2119–2151, 2013

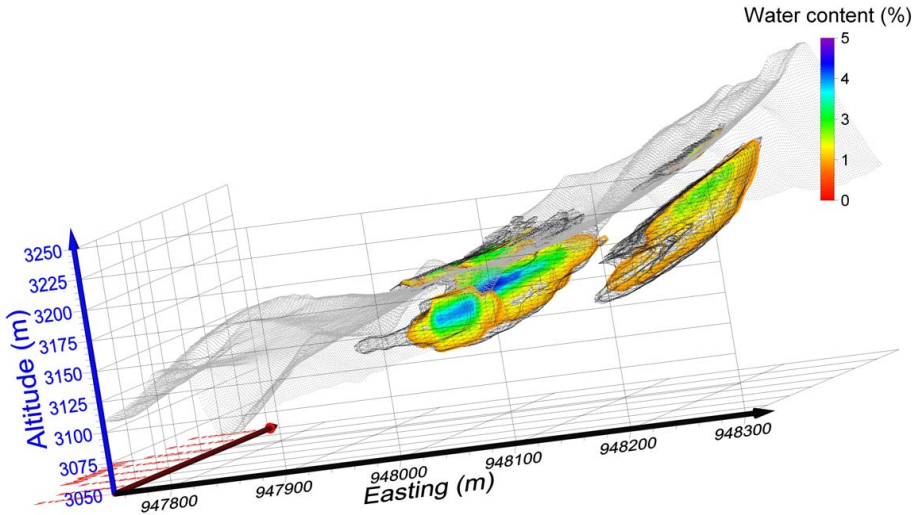

Fig. 11. 3-D-SNMR image of the water-filled cavern observed in October 2012. The glacier surface is shown as a gray sheet.

TCD
7, 2119–2151, 2013